Wavelet-basis calculation of Wannier functions

Stephen D. Clow and Bruce R. Johnson
Department of Chemistry and Rice Quantum Institute, MS 600, Rice University, Houston, Texas 77005-1892, USA
(Received 31 July 2003; published 15 December 2003)

Wannier functions for a one-dimensional quantum system with a generic periodic potential are calculated directly using orthogonal compact support multiwavelets in conjunction with a sparse iterative method. This allows systematic elimination of error from scales both shorter and longer than the basic period. The converged values of the Wannier function and the associated energy Fourier components are analyzed, yielding improved formulas for their behavior in the important regions that are not fully asymptotic.

DOI: 10.1103/PhysRevB.68.235107 PACS number(s): 71.15.Ap, 02.70.−c, 71.15.Dx

I. INTRODUCTION

In systems with periodic potentials, the Bloch-Floquet wave functions may be expanded in a Fourier series of Wannier functions, each of which is centered around a particular site.[1,2] The Wannier functions possess greater localization and can form useful alternative quantum bases for the description of, e.g., electrons in insulating crystals,[1] crystal defects,[3] surfaces,[4] wave propagation in photonic crystals,[5] and properties of optically trapped Bose-Einstein condensates[6,7] (from which bright matter-wave soliton trains have now been created and observed[8]). It has long been known that Wannier functions for systems with a nonzero gap exhibit exponential decay $\exp(-h|\mathbf{R}-\mathbf{R}_0|)$ with distance from their central sites in either one[2] or higher[9] dimensions. It is only very recently, however, that He and Vanderbilt[10] have discovered power-law prefactor corrections to this simple asymptotic behavior for the Wannier functions, energy Fourier series, and density matrix for a one-dimensional (1D) model potential. Taraskin *et al.*[11] have since characterized the density matrix corrections for a tight-binding model on simple cubic lattices in 1D, 2D, and 3D. Electronic structure calculations of Wannier functions for realistic crystals are also of strong current focus,[12–16] particularly from the standpoint of linear scaling methods.[17] Analysis of the asymptotic behavior of the latter results can be complicated by their multidimensional character, by possible limitations of the atomic/molecular basis sets, by possible limitations from truncation of the number of unit cells included, and, we now know, by expected modifications to simple exponential falloff in the incompletely asymptotic regime relevant to local numerical calculations. This last aspect is pursued quantitatively here for the simplest case of a 1D simple band using the results of He and Vanderbilt,[10] who also point out the existence of higher-order corrections to the prefactors. One can define a fully asymptotic distance regime in which all such higher-order corrections are negligible to within a chosen numerical threshold. At shorter distance is an intermediate regime in which the asymptotic expansion augmented by higher-order corrections provides a reliable description of the Wannier functions. At the shortest distances (generally one to several unit cells), the correction terms do not even exhibit limited convergence, and so numerical computations are required. This paper examines the quantitative improvement of the asymptotic expansion obtained in the intermediate distance regime by explicitly including the next leading orders in the prefactor. Going further, analytical formulas are derived for the energy Fourier components and Wannier functions that have improved accuracy at intermediate distances.

The results are judged by numerical calculation of the Wannier function in a way that can systematically reduce both basis set and truncation error. While one can use the indirect method of Fourier transforming the Bloch function (Brillouin zone integration), direct methods using localized basis functions to calculate the localized Wannier function in real space were long ago advocated by Kohn[18] and undergo continued development. Wavelet bases possessing orthogonality are of interest in this context, especially since in many cases they share the Wannier function motif: neighboring functions are orthogonal even though they overlap spatially. In fact, the Wannier functions *are* particular types of wavelets in the limit that the potential vanishes.[19] Wavelets with orthogonality and compact support[20] have already formed the basis for a wide variety of digital applications in signal and image processing.[21] It has been a goal of more recent investigations to establish that orthogonal compact support wavelets can be used with high accuracy in prototypical quantum problems, e.g., a deep double-well potential,[22,23] the particle in a box,[24] the hydrogen atom[24,25] and the hydrogen molecular ion.[26] (Other types of wavelets have been utilized in quantum applications as well.[27–29]) In the case of Wannier functions, which satisfy a well-known differential equation derived by Parzen[30] and Koster,[31] an orthogonal wavelet basis provides a representation with matrices of a particular sparse character. This suggests the use of methods relying upon efficient matrix-times-vector multiplication operations. In the following, an iterative method is developed for which the central computational step scales linearly with basis size N. It is expected that this direct numerical procedure will generalize to more complicated scenarios than the 1D simple band (e.g., realistic crystals, entangled bands, multidimensional optical trapping), although the latter is the focus of the present investigation. In this case one can quantify to how short a distance the asymptotic expansions provide a useful description of the Wannier function and energy components. From a practical standpoint of postanalysis of numerical calculations, it is to be hoped that more detailed descriptions can be developed of the closer regions where Wannier func-

tions are usually calculated and joined to the asymptotic expansions.

II. WANNIER FUNCTIONS

For a simple energy band of a 1D Hamiltonian $\hat{H}$ with a periodic potential, the Bloch/Floquet eigenfunction $b_k(x)$ is spread over the entire lattice. For simplicity, it is assumed that the cells have unit spacing. The function $b_k(x)$ may be expanded in a Fourier series

$$b_k(x)=(2\pi)^{-1/2}\sum_{n=-\infty}^{\infty} e^{ikn}w(x-n), \tag{1}$$

with Wannier functions as components,

$$w(x-n)=(2\pi)^{-1/2}\int_{-\pi}^{\pi} e^{-ikn}b_k(x)dk. \tag{2}$$

The function $w(x-n)$ is centered around site n, decays in magnitude with increasing distance from $x=n$, and is orthogonal to those centered around other sites $n'\neq n$. Similarly, the Bloch eigenvalue E_k can be expanded as

$$E_k=\sum_{n=-\infty}^{\infty} e^{ikn}\varepsilon_n, \tag{3}$$

$$\varepsilon_n=(2\pi)^{-1}\int_{-\pi}^{\pi} e^{-ikn}E_k dk. \tag{4}$$

As discussed by Parzen[30] and Koster,[31] the Wannier functions satisfy the differential equation

$$\hat{H}w(x)=\sum_n \varepsilon_n w(x-n)=\sum_n \varepsilon_n \hat{D}_n w(x), \tag{5}$$

where $\hat{D}_n$ is a displacement operator corresponding to translation by n unit cells. From the orthonormality of the different $w(x-n)$, the energy Fourier components can be expressed as

$$\varepsilon_n=\int w^*(x)\hat{H}w(x-n)dx. \tag{6}$$

In the limit of strongly bound levels, the ε_n for $n\neq 0$ are very small, $w(x)$ is confined to the $n=0$ cell, and ε_0 is an ''atomic'' eigenvalue. More generally, we may still regard Eq. (5) as an eigenvalue equation for ε_0, while the other ε_n serve as Lagrange multipliers whose values affect the degree of orthogonality between a calculated $w(x)$ and its translated copies.

The analysis by Kohn[2] for a 1D centrosymmetric crystal with a periodic potential established that the Wannier function decays as $e^{-h|x|}$ for large $|x|$, where the value of the constant h is determined by the location of branch points of the Bloch energy in the complex k plane. The energy components ε_n correspondingly decay as $e^{-h|n|}$ with the same constant h. He and Vanderbilt[10] have now established more precise behaviors, $w(x)\sim|x|^{-3/4}e^{-h|x|}$ and $\varepsilon_n\sim|n|^{-3/2}e^{-h|n|}$, with the prefactors determined by the behaviors of $b_k(x)$ and E_k near the branch points. A periodic Gaussian potential $\Sigma_n V(x-n)$ where $V(x)=(V_0/b\sqrt{\pi})e^{-x^2/b^2}$ was used as a particular example to represent the general case (no analytical solutions are available). The present numerical wavelet methods are tested on the same potential, adopting the earlier choices of atomic units, potential parameters $V_0=-10$, $b=0.3$, and focus on the lowest-energy band, leading to a decay parameter $h=1.288\,69$.

Calculations of Wannier functions, usually performed for crystals, frequently start with exponentially localized atomic or bond orbitals as trial functions. As described by Kohn,[18] these may be orthonormalized among neighboring cells by the methods of des Cloizeaux[9] or Löwdin[32] while maintaining identical shapes from one site to the next. The Wannier functions are then obtained from the orthonormal basis by variation of the orbital parameters to find a stationary expectation value for $\hat{H}$.[3,33] There is usually some error associated with incompleteness of the atomic or molecular basis set, although this is generally difficult to precisely assess or systematically reduce. Further errors may come from the necessity of using a finite number of cells in the calculations, although this truncation error is more amenable to systematic study. These same issues may apply to the need for calculation of Wannier functions for general periodic systems other than crystals.[7] Systematic studies can be implemented through plane wave methods, although local methods such as finite elements or wavelets offer the possibility of customizable resolution. Wavelets offer the additional choice of orthogonal bases (a convenience though not a necessity) and so an exploration into their use for calculation of a Wannier function is undertaken here.

III. MULTIWAVELET BASIS

A compact support wavelet basis consists of strictly localized functions indexed by location and scale. The most well-known families are those due to Daubechies[20] in which all functions are shifted and scaled duplicates of a single father wavelet (or scaling function) and a single mother wavelet. Such families necessarily have skewed shapes[20] which introduce an inconvenient left-versus-right bias. We instead use a multiwavelet family derived by Chui and Lian, consisting of symmetric and antisymmetric pairs of father and mother wavelets orthogonal on the interval [0,3].[34] The scaling functions and their shifted neighbors are shown in Fig. 1, all functions shown being mutually orthogonal and providing an exact expansion basis for piecewise polynomial functions up to quadratic order. While multiwavelet applications to quantum mechanics are still rare, some demonstrations have now appeared.[24,26,35]

The multiscaling functions on different octaves have the simple unit-normalized forms

$$\phi_{jk\alpha}(x)=2^{j/2}\phi_\alpha(2^j x-k) \tag{7}$$

for integer j and k, with $\alpha=1$ corresponding to the symmetric functions and $\alpha=2$ to the antisymmetric functions. The $\phi_{jk\alpha}(x)$ are nonzero only on the support intervals $k2^{-j}\leqslant x$

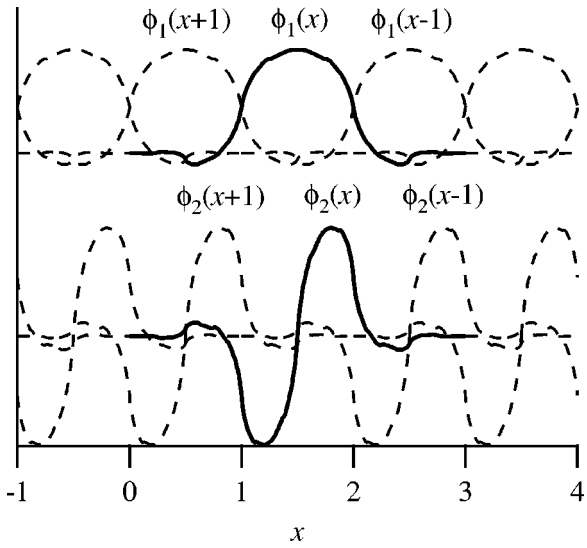

FIG. 1. Symmetric and antisymmetric Chui-Lian multiscaling functions orthogonal on the interval [0,3] (solid lines) and translated copies (dashed lines).

$\leqslant (k+3)2^{-j}$. For a single fixed j, the Wannier function may be approximated as a finite orthonormal expansion

$$w(x) \cong \sum_{k=k_{\min}}^{k_{\max}} \sum_{\alpha=1}^{2} u_{jk\alpha} \phi_{jk\alpha}(x), \tag{8}$$

where j controls the resolution and $\{k_{\min}, k_{\max}\}$ control the range. These are to be determined, respectively, by the dynamical variation and effective extent of $w(x)$, the latter being correlated with the decay parameter h. One may also use the equivalent multiresolution basis consisting of coarser scaling functions and the associated mother wavelets across a number of different scales, although this is not a primary issue in the current investigation.

The solution of Eq. (5) via this basis requires efficient methods for the evaluation of matrix elements. For different choices of j, the basis functions are (by construction) related via two-scale relations[34]

$$\phi_{jk\alpha}(x) = 2^{-1/2} \sum_{k'=0}^{3} \sum_{\alpha'=1}^{2} c_{k'\alpha\alpha'} \phi_{j+1,2k+k',\alpha'}(x), \tag{9}$$

where the $\mathbf{c}_{k'}$ are 2×2 constant matrices. These relations may be used in reducing the calculation of matrix elements of $-(d/dx)^2/2$ to the solution of simple linear equations.[24,36] In practice, a regularized form of the kinetic energy matrix has been found to offer superior performance,[24] in loose analogy with the use of higher-order formulas in finite difference calculations, and is adopted here.

Matrix elements of x^n can be evaluated similarly and then used to develop numerical quadrature formulas for matrix elements of general potentials, the maximum absolute error decreasing exponentially with increasing resolution j.[24,37] Using uniformly spaced samples of the potential, the number of potential evaluations is kept essentially linear in the number of basis functions, providing high efficiency. Accuracy can be controlled by performing the quadrature on finer scales $J > j$ and using the two-scale relations in Eq. (9) on both bra and ket functions in the integrals to provide exponentially refined estimates at level j. The starting level J can be systematically increased until convergence to any prespecified level is obtained. To eliminate any possible issues of errors in potential matrix elements, these were calculated once in MATHEMATICA (Wolfram Research) using extended precision and stored, all desired matrix elements being converged to better than one part in 10^{18}.

Due to the localized nature of the basis, the Hamiltonian matrix $\mathbf{H}$ takes a symmetric banded form with five subdiagonals and five superdiagonals when the basis functions are organized in a 1D array $\ldots, \phi_{jk1}, \phi_{jk2}, \phi_{j,k+1,1}, \phi_{j,k+1,2}, \ldots$. The translation operators on the right-hand side of Eq. (5) require intercell overlap integrals which are exceedingly simple for the wavelet basis

$$\int \phi_{jl\beta}(x) \hat{D}_n \phi_{jk\alpha}(x) dx = \int \phi_{jl\beta}(x) \phi_{j,k+2^j n,\alpha}(x) dx = \delta_{l,k+2^j n} \delta_{\beta\alpha}. \tag{10}$$

Thus the additional terms lead only to multiples of $\mathbf{D}_n$, a unit off-diagonal matrix separated by $2^{j+1}n$ from the main diagonal. Since $E_{-k} = E_k$ in the symmetric example under consideration, we also have from Eq. (3) that $\varepsilon_{-n} = \varepsilon_n$. The matrix of interest is therefore the symmetric matrix

$$\overline{\mathbf{H}} = \mathbf{H} - \sum_{n>0}^{n_{\max}} \varepsilon_n (\mathbf{D}_{-n} + \mathbf{D}_n), \tag{11}$$

for which an efficient matrix-vector multiply algorithm can be constructed using the matrix $\mathbf{H}$ stored in packed form and simple shift operations for the extra terms. The lowest eigenvalue ε_0 and its associated eigenvector can be sought using sparse matrix techniques, but only if one has knowledge of the other ε_n.

IV. ITERATIVE WANNIER FUNCTION CALCULATION

To determine the Lagrange multipliers ε_n, $n>0$, simultaneously with ε_0 and $w(x)$, a suitable iterative procedure has been developed which allows resolution to be increased in stages. For a fixed initial level j_0 (which may be zero), one starts with a trial vector $\mathbf{u}_0$ symmetrically localized around the central cell and with all ε_n for $n>0$ set to zero. The steps are then as follows. (i) A vector $\mathbf{u}_1 = (\mathbf{u}_0 + \beta \overline{\mathbf{H}} \cdot \mathbf{u}_0)/\|\mathbf{u}_0 + \beta \overline{\mathbf{H}} \cdot \mathbf{u}_0\|$ is calculated with β chosen to minimize $\mathbf{u}_1^T \cdot \overline{\mathbf{H}} \cdot \mathbf{u}_1$. (ii) The Löwdin symmetric orthogonalization process[32] is iterated starting from $\mathbf{u}_1$, producing a new symmetric vector $\mathbf{u}_2$ orthogonal to its translations $\mathbf{u}_{2,n} = \mathbf{D}_n \cdot \mathbf{u}_2$. (iii) The latter vectors are used to calculate improved estimates $\varepsilon_n = \mathbf{u}_2^T \cdot \mathbf{H} \cdot \mathbf{u}_{2,n}$ according to Eq. (6). Then $\mathbf{u}_0$ is overwritten with $\mathbf{u}_2$ and steps (i)–(iii) are repeated with the updated ε_n. The range of basis functions included is chosen so that $n_{\max}$ unit cells are spanned on either side, $n_{\max}$ being determined according to the falloff found in the calculations. All ε_n parameters for the target number of unit cells are determined at one time, each individual cell being treated with a degree of

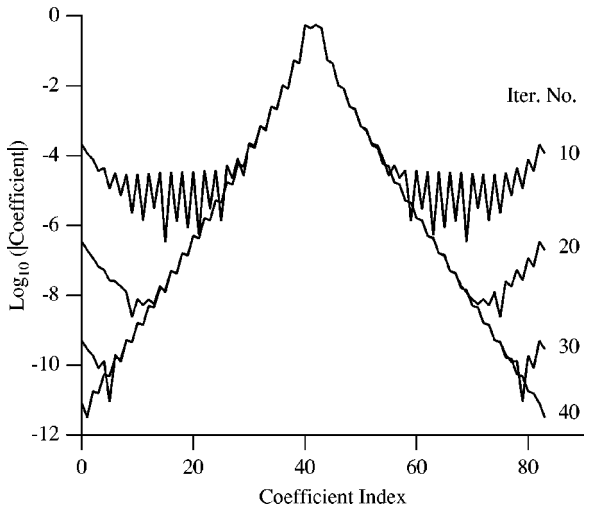

FIG. 2. Convergence of the magnitudes of the Wannier function coefficients in the Chui-Lian $j=0$ scaling function basis with number of iteration steps. There are two coefficients per unit cell on this scale.

resolution determined by the fineness of the basis used. It can be recognized that step *i* above is basically a lowest-order restarted Lanczos procedure, suggesting possible refinements of the method to be explored in the future.

Figure 2 demonstrates convergence of the coefficients after 10, 20, 30, and 40 iterations using $j=0$ and $n_{\max}=20$. The apparent slight asymmetry is due to the use of the same ordering (symmetric before antisymmetric) for basis functions on both left and right. Convergence is rapid and the converged coefficients decay approximately exponentially in magnitude with distance from the central cell. Timings have been determined for 50 iteration steps with $n_{\max}=20$, using MATHEMATICA in 30-digit precision on an 850 MHz linux machine. The initial resolution was varied over the range $j_0=0-6$ and the corresponding basis sizes were chosen to be 84×2^{j_0} for simplicity of comparison. The CPU times for successive j_0 were found to be 35, 68, 139, 279, 581, 1228, and 2922 s. Except for the largest bases (which may be affected by, e.g., cache dependency) the basic iteration steps scale linearly with basis size.

With increasing basis size, of course, the calculated $w(x)$ and ε_n converge more slowly. This can be partially compensated by starting from low resolution where convergence is rapid and proceeding to higher resolution in steps (similar to multigrid philosophy). The two-scale recursions in Eq. (9) are used to express the level j basis functions in terms of those from level $j+1$, providing a well-adapted starting vector for the latter and expediting the iteration process. The scale refinement was carried out to $j=6$ to ensure convergence with respect to intracell detail and to $n_{\max}=32$ to ensure elimination of truncation error for all but the most distant cells.

In view of the large dynamic range of the Wannier function, the graphs in Fig. 3 factor the dominant asymptotic behavior[10] $w(x)\propto x^{-3/4}e^{-hx}(x>0)$ from the numerical results. It is seen in Fig. 3(a) that this indeed yields a continuous sequence of nearly uniform oscillations. The segments

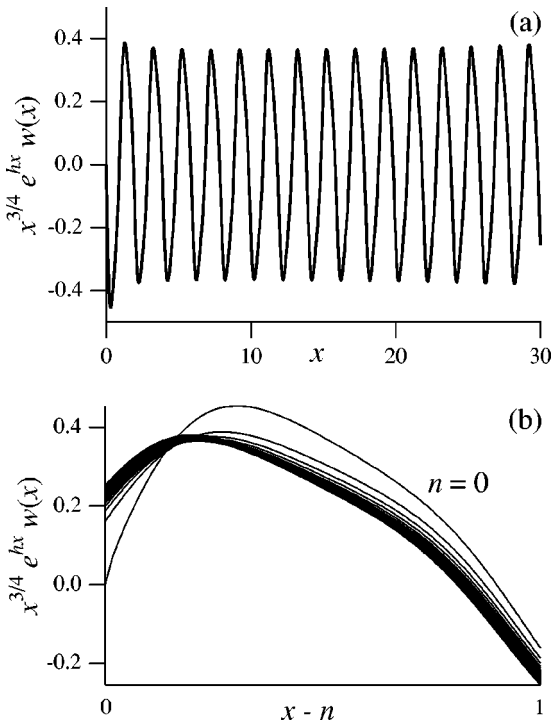

FIG. 3. (a) Wannier function $w(x)$ times $x^{3/2}e^{hx}$; (b) overlay of $w(x)$ times $(-1)^{n+1}x^{3/2}e^{hx}$ in the various intervals $n\leqslant x\leqslant n+1$, $n<30$.

on each interval $n\leqslant x\leqslant n+1$ (multiplied by -1 for n even) are shown overlapped in Fig. 3(b). These figures are not sensitive to use of the $j=5$ Wannier function or to small changes in the value of h.

The values of the ε_n are given in Table I for both $j=5$ and 6 with $n_{\max}=32$ and for $j=6$ with $n_{\max}=33$. One finds scale convergence to $\sim$10 significant figures for $n=0$. For $n=30$, scale convergence is to $\sim$5 significant figures, but $n_{\max}$ convergence is only to $\sim$4. Comparison of the results for $n=31$ and 32 demonstrates the general result that the ε_n for the highest pair of values of n are always the most sensitive to change of $n_{\max}$ and incompletely converged. Figure 4 factors out the dominant asymptotic behavior $|\varepsilon_n| \propto n^{-3/2}e^{-hn}$, showing that even the energy components are somewhat slow in reaching their asymptotic forms.

From the results of He and Vanderbilt, it is expected that $w(x)$ and ε_n possess higher-order subdominant corrections,

$$w(x)=W_0(x)x^{-3/4}e^{-hx}+W_1(x)x^{-5/4}e^{-hx} + W_2(x)x^{-7/4}e^{-hx}+\cdots, \tag{12}$$

$$\varepsilon_n=a_0n^{-3/2}e^{-hn}+a_1n^{-5/2}e^{-hn}+\cdots, \tag{13}$$

in terms of bounded functions $W_i(x)$ and constants a_i. Noting the alternation in sign of the ε_n, least squares fits excluding the first few values were made to the corrected form

$$\varepsilon_n\approx(-1)^nC(n^{-3/2}+\gamma n^{-5/2})e^{-hn}, \tag{14}$$

with $C=1.451\,17$, $h=1.288\,69$, and $\gamma=0.276\,22$. This value of h agrees with that of He and Vanderbilt, although the last

TABLE I. Convergence of ε_n as calculated via wavelet iteration with increasing resolution. Numbers in brackets indicate powers of 10.

n	$j=5$, $n_{\max}=32$	$j=6$, $n_{\max}=32$	$j=6$, $n_{\max}=33$
0	−10.719133737	−10.719133742	−10.719133742
1	−4.964710109[−1]	−4.964710102[−1]	−4.964710102[−1]
2	4.403635305[−2]	4.403635295[−2]	4.403635295[−2]
3	−6.368236336[−3]	−6.368236315[−3]	−6.368236315[−3]
4	1.117802084[−3]	1.117802079[−3]	1.117802079[−3]
5	−2.177573562[−4]	−2.177573549[−4]	−2.177573550[−4]
6	4.527573596[−5]	4.527573558[−5]	4.527573562[−5]
7	−9.842592752[−6]	−9.842592636[−6]	−9.842592651[−6]
8	2.210171168[−6]	2.210171131[−6]	2.210171137[−6]
9	−5.086700132[−7]	−5.086700003[−7]	−5.086700029[−7]
10	1.193569301[−7]	1.193569255[−7]	1.193569266[−7]
11	−2.844680672[−8]	−2.844680503[−8]	−2.844680545[−8]
12	6.867483317[−9]	6.867482690[−9]	6.867482856[−9]
13	−1.675848583[−9]	−1.675848351[−9]	−1.675848415[−9]
14	4.127086684[−10]	4.127085826[−10]	4.127086067[−10]
15	−1.024399810[−10]	−1.024399496[−10]	−1.024399586[−10]
16	2.560156079[−11]	2.560154938[−11]	2.560155268[−11]
17	−6.436805265[−12]	−6.436801165[−12]	−6.436802360[−12]
18	1.626972535[−12]	1.626971076[−12]	1.626971504[−12]
19	−4.131846864[−13]	−4.131841725[−13]	−4.131843236[−13]
20	1.053779264[−13]	1.053777471[−13]	1.053777999[−13]
21	−2.697833770[−14]	−2.697827573[−14]	−2.697828999[−14]
22	6.930786231[−15]	6.930804721[−15]	6.930810981[−15]
23	−1.786175571[−15]	−1.786168370[−15]	−1.786170494[−15]
24	4.616523541[−16]	4.616499312[−16]	4.616506460[−16]
25	−1.196339942[−16]	−1.196331859[−16]	−1.196334242[−16]
26	3.107791374[−17]	3.107764627[−17]	3.107772515[−17]
27	−8.091447128[−18]	−8.091359357[−18]	−8.091385461[−18]
28	2.111084371[−18]	2.111055981[−18]	2.111065568[−18]
29	−5.518497377[−19]	−5.518415674[−19]	−5.518502963[−19]
30	1.444795380[−19]	1.444822518[−19]	1.445175000[−19]
31	−3.762851456[−20]	−3.766394864[−20]	−3.790320580[−20]
32	6.849229839[−21]	7.197616212[−21]	9.910638518[−21]
33			−2.047015812[−21]

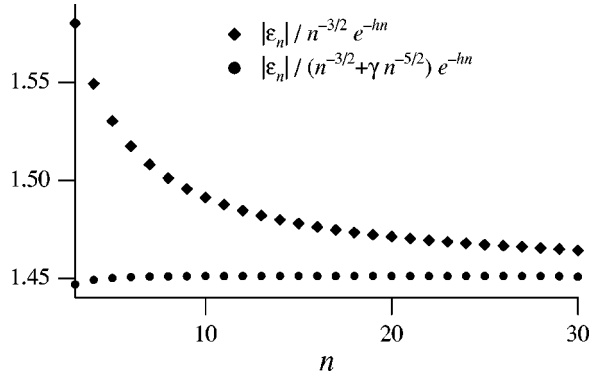

FIG. 4. Magnitudes of the ε_n after factoring out the dominant asymptotic behavior with and without an $n^{-5/2}$ correction.

digit is slightly dependent on the exact choice of the ε_n used. The quality of the latter fit is evident from the near-constant nature of the ε_n after factoring of the n dependence, as displayed in Fig. 4. The correction terms are therefore concluded to be significant in the quantitative analysis of the numerical results, particularly in the region of intermediate n.

V. HIGHER-ORDER CORRECTIONS

The corrections beyond those of leading order can be evaluated by extension of Kohn's analysis for the 1D case.[2] Two fundamental solutions $\psi_1(x,E)$ and $\psi_2(x,E)$ to the Schrödinger equation for the periodic potential are defined by the boundary conditions $\psi_1(0,E)=1$, $\psi_1'(0,E)=0$ and $\psi_2(0,E)=0$, $\psi_2'(0,E)=1$ for general complex E. A central role is played by the quantity $\mu(E)=\psi_1(1,E)$, an entire function of E whose derivative $d\mu/dE$ vanishes at real val-

ues $E=E_m$, $m=0,1,...$, outside the allowed ranges of E. For the ground state ($m=0$), we have $\mu_0<-1$ and, for E close to E_0,

$$\mu(E)=\mu_0+\alpha_0(E-E_0)^2+\beta_0(E-E_0)^3+\gamma_0(E-E_0)^4+\cdots. \quad (15)$$

Inversion of the series yields

$$E=E_0\pm\alpha_0^{-1/2}(\mu-\mu_0)^{1/2}-\beta_0\alpha_0^{-2}(\mu-\mu_0)\pm\frac{1}{8}(5\beta_0^2-4\alpha_0\gamma_0)\alpha_0^{-7/2}(\mu-\mu_0)^{3/2}+\cdots, \quad (16)$$

the lower sign being taken here. With the identification[2] $\mu=\cos(k)$, one has an expression for E as a function of k which may be used in the Fourier integral of Eq. (4) to obtain the ε_n. It is immediately evident that the constant terms in Eq. (16) contribute only for $n=0$ and the term linear in μ contributes only for $n=\pm1$. Analogously, if terms in $(\mu-\mu_0)^2$ were retained, these would contribute only for $|n|\leqslant 2$, etc.

The nonvanishing contributions to ε_n for higher n come from the radical terms. These may be evaluated using a contour deformation in the complex k plane introduced by He and Vanderbilt. As functions of complex E, μ, and k, each of the radicals has two-sheeted branch points at values $k_0=\pi\pm ih_0$ (as well as others). The distance from the real k axis is $h_0=\cosh^{-1}(-\mu_0)>0$ (the decay parameter h discussed earlier). Focusing on the upper branch point and introducing $\Delta k=k-k_0$, complex trigonometric identities give

$$\mu-\mu_0=\mu_0(\cos\Delta k-1)+i(\mu_0^2-1)^{1/2}\sin\Delta k. \quad (17)$$

In the limit of small Δk, we find $E-E_0\propto(k-k_0)^{1/2}$ as described by Kohn. Deforming to a contour C_1 starting at $\pi+i\infty$ on one Riemann sheet, running around the branch point $k_0=\pi+ih_0$, and ending at $\pi+i\infty$ on the other sheet, Fourier integrals of $(k-k_0)^\nu$ are mapped exactly into products of gamma functions and factors $n^{-1-\nu}$ as exhibited in Eq. (13).[10]

This same contour deformation can be used to advantage even if one does not make a small Δk approximation in Eq. (17). One finds for $n>\nu$ that

$$\oint_{C_1}(\mu-\mu_0)^\nu e^{ikn}dk=-2e^{ik_0n}I_\nu(n), \quad (18)$$

$$I_\nu(n)=\sin(\pi\nu)\int_0^\infty[-\mu_0(\cosh\kappa-1)+(\mu_0^2-1)^{1/2}\sinh\kappa]e^{-\kappa n}d\kappa, \quad (19)$$

using the change of variables $k-k_0=i\kappa$. Truncating the expansion in Eq. (16), we therefore obtain

$$\varepsilon_n\approx\frac{1}{\pi}e^{ik_0n}\left[\alpha_0^{-1/2}I_{1/2}(n)+\frac{1}{8}(5\beta_0^2-4\alpha_0\gamma_0)\alpha_0^{-7/2}I_{3/2}(n)\right], \quad (20)$$

where the prefactor $e^{ik_0n}=(-1)^ne^{-h_0n}$ contains both the sign alternation and the exponential decay with n. For $n\leqslant\nu$, the integral in Eq. (19) fails to converge, indicating that the expansion in Eq. (16) is then an inappropriate means of evaluating ε_n. All results below apply only to n greater than the maximum power of $\mu-\mu_0$ retained in the truncation.

Using the fact that

$$-\mu_0\pm(\mu_0^2-1)^{1/2}=e^{\pm h_0}, \quad (21)$$

the integral in Eq. (19) can be evaluated analytically for $-1<\nu<n$ in terms of beta and hypergeometric functions,[38]

$$I_\nu(n)=\sin(\pi\nu)2^\nu\int_0^\infty\left[\sinh\left(\frac{\kappa}{2}\right)\sinh\left(\frac{\kappa}{2}+h_0\right)\right]^\nu e^{-\kappa n}d\kappa$$
$$=\sin(\pi\nu)2^{-\nu}e^{h_0\nu}B(n-\nu,\nu+1)\ {}_2F_1(n-\nu,-\nu,n+1,e^{-2h_0}). \quad (22)$$

Different regimes of behavior for the ε_n are contained in this result. For h_0 not close to zero ($\mu_0\neq-1$) and $n\gg1$, the beta function $\sim\Gamma(\nu+1)n^{-1-\nu}$ and the hypergeometric function $\sim(1-e^{-2h_0})^\nu$, leading to the previous result,

$$I_\nu(n)\approx\sin(\pi\nu)(\mu_0^2-1)^{\nu/2}\Gamma(\nu+1)n^{-1-\nu}. \quad (23)$$

This is also obtainable by taking $\cosh\kappa\to1$ and $\sinh\kappa\to\kappa$ in Eq. (19), recognizing that only small values of κ contribute to the integration for large n. For small n and large h_0, the hypergeometric function is close to unity, and the n dependence of Eq. (22) is dominantly given by the ratio $\Gamma(n-\nu)/n!$

In the weak-binding limit, we have $\mu_0\approx-1$, $h_0\approx0$ and $e^{-2h_0}\approx1$, leading to

$$I_\nu(n)\approx\sin(\pi\nu)2^{-\nu}e^{h_0\nu}B(n-\nu,\nu+1)\times\frac{\Gamma(n+1)\Gamma(1+2\nu)}{\Gamma(1+\nu)\Gamma(n+1+\nu)}$$
$$\approx\sin(\pi\nu)2^{-\nu}B(n-\nu,2\nu+1), \quad (24)$$

which decays approximately as $n^{-2\nu-1}$. The asymptotic falloff of ε_n is then $e^{-h_0n}n^{-2}$, with the n^{-2} behavior (the behavior expected for a free particle) dominating for $n<1/h_0$.

Moving somewhat away from the weak-binding limit, the hyperbolic trigonometric functions may be expanded up to quadratic terms in Eq. (19) to obtain another approximate analytic description of the integrals,

$$I_\nu(n)\approx\sin(\pi\nu)\int_0^\infty[-\mu_0\kappa^2+(\mu_0^2-1)^{1/2}\kappa]\exp(-\kappa n)d\kappa$$
$$=\sin(\pi\nu)(2/\pi)^{1/2}\Gamma(\nu+1)\times(-\mu_0)^\nu(u/n)^{\nu+1/2}e^{un}K_{\nu+1/2}(un). \quad (25)$$

The linear term always dominates in the integration if $u=(\mu_0^2-1)^{1/2}/|\mu_0|\gg1/n$, leading again to terms behaving as $n^{-\nu-1}$, $n^{-\nu-2}$, etc., as may be verified by asymptotics of the Bessel function. For $\nu=1/2$ and low n, one also finds from

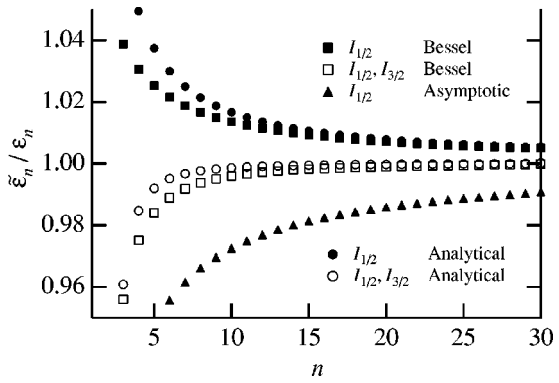

FIG. 5. Ratios of different approximations $\tilde{\varepsilon}_n$ to converged values of ε_n.

this expression a dominant behavior n^{-2}, although there are some errors in the coefficients since higher ranges of κ contribute significantly to the integration and the effects of the truncation inside the integrand are more strongly felt. For intermediate n, there is a crossover region between the two behaviors, consistent with the observation by He and Vanderbilt[10] of a crossover region in the Wannier function between x^{-1} falloff at low x and $x^{-3/4}e^{-h_0 x}$ falloff at large x. This crossover region was found to move to larger x as the binding weakened, in agreement with the movement of the ε_n crossover region to larger n as u decreases.

In order to assess the above approximations, the Schrödinger equation for the fundamental solution $\psi_1(x,E)$ was integrated by the Runge-Kutta method from $x=0$ to $x=1$. The energy E was varied until $\mu=\psi_1(1,E)$ reached its extremum μ_0, leading to the accurate value $h_0=1.288\,667\,130\,49$. (This value differs slightly from the results of He and Vanderbilt and our own approximate fit above, so the extended-precision result was double checked for procedure and convergence.) Numerical differentiation then yielded for the constants in Eq. (15) the values $\alpha_0=0.063\,445\,354\,69$, $\beta_0=0.006\,066\,649\,65$, and $\gamma_0=0.000\,253\,868\,90$. Figure 5 shows $\tilde{\varepsilon}_n/\varepsilon_n$ where ε_n is calculated via the iterative wavelet algorithm and $\tilde{\varepsilon}_n$ is calculated under different approximations: the asymptotic $n^{-3/2}e^{-h_0 n}$ form from Eq. (23), the analytical formula of Eq. (22) with and without $I_{3/2}$, and the Bessel approximation of Eq. (25) with and without $I_{3/2}$. It is clear that inclusion of $I_{3/2}$ dramatically improves the accuracy over all but the lowest values of n and that the simple Bessel approximation is only marginally worse than the hypergeometric expression. The residual errors at low n are expected to arise chiefly from the limitations of using the truncated asymptotic expansion in Eq. (16) to represent the inverted function $E(\mu)$. Nevertheless, Fig. 5 makes it clear that the above results with higher-order corrections (and no adjustable parameters) provide significantly improved approximations over the rest of the range of n.

The integrals above are also useful in description of the Wannier function, although the higher-order corrections are more complicated. The Bloch function as described by Kohn takes the form

$$b(x,E)=N(E)^{-1/2}[\chi_1(x,E)+\chi_2(x,E)]=N(E)^{-1/2}\chi(x,E), \tag{26}$$

$$\chi_1(x,E)=\psi_2(1,E)\psi_1(x,E), \tag{27}$$

$$\chi_2(x,E)=(\mu^{2-1})^{1/2}\psi_2(x,E). \tag{28}$$

The normalization constant is an analytic function of complex E defined by

$$N(E)=2\pi\int_0^1[\chi_1(x,E)+\chi_2(x,E)][\chi_1(x,E)-\chi_2(x,E)]dx$$

$$=-2\pi\psi_2(1,E)\frac{d\mu}{dE}, \tag{29}$$

which vanishes at $E=E_0$ in the forbidden energy region. [The last form differs from that derived by Kohn by a factor of 1/2 due to the choice of $-1/2(d/dx)^2$ rather than $-(d/dx)^2$ in the Schrödinger equation.] The precise behavior of the wave function around this branch point depends on the local behaviors of both $N(E)$ and $\chi(x,E)$. Exceptional cases in which $\psi_2(1,E)$ vanishes lead to compensating behavior in $\chi(x,E)$, as discussed in detail by Kohn.

Expanding both N and χ through two orders of nonvanishing terms,

$$b(x,E)\cong[N'(E_0)\Delta E+N''(E_0)\Delta E^2/2]^{-1/2}\left[\chi(x,E_0)+\frac{\partial\chi}{\partial E}(x,E_0)\Delta E\right]\cong[-\alpha_0^{-1/2}N'(E_0)]^{-1/2}(\mu-\mu_0)^{-1/4}\chi(x,E_0)$$
$$+[-\alpha_0^{-1/2}N'(E_0)]^{-1/2}\left[\frac{\beta_0}{2\alpha_0^{3/2}}+\frac{N''(E_0)}{4\alpha_0^{1/2}N'(E_0)}\right](\mu-\mu_0)^{1/4}\chi(x,E_0)$$
$$-[-\alpha_0^{-1/2}N'(E_0)]^{-1/2}(\mu-\mu_0)^{1/4}\left[\alpha_0^{-1/2}\frac{\partial\chi}{\partial E}(x,E_0)\right]. \tag{30}$$

All of the dependence on n in the Fourier transformation of this expression arises through the integrals over powers of $\mu-\mu_0$ given above. Knowledge of $\chi(x,E_0)$ and its energy derivative on the interval $0\leqslant x\leqslant 1$ combined with values of $I_\nu(n)$ for $\nu=\pm 1/4$ therefore allows approximate evaluation of $w(x)$ on the interval $n\leqslant x\leqslant n+1$. Figure 6 shows the ratio

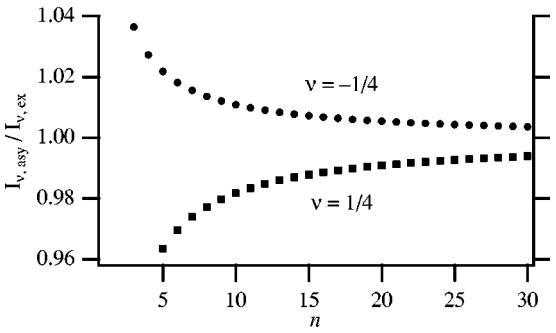

FIG. 6. Ratio of integrals I_v calculated by the asymptotic Eq. (23) to the exact results of Eq. (22).

of the asymptotic $I_\nu(n)$ from Eq. (23) to the exact $I_\nu(n)$ from Eq. (22). The latter form is used in the Wannier function examples of Fig. 7 for $n=5$ and 10. It is seen that use of the $(\mu-\mu_0)^{-1/4}$ term already gives reasonably good agreement, but that inclusion of the $(\mu-\mu_0)^{1/4}$ term improves agreement over all regions except right at the peaks. The agreement in the mid-n ranges of Fig. 7 is quite reasonable and, again, is obtained without any adjustable parameters.

The convergence with powers of ν is naturally expected to be slower for the Wannier function than for the energy components since the powers increase only by 1/2 at each step. Higher-order corrections were therefore examined by carrying the expansions to $\nu=3/4$ and 5/4 powers of $\mu-\mu_0$, but herein lies a problem. While these two contributions partially cancel in the Wannier function expression, they are individually intermediate in magnitude between the $\nu=\pm 1/4$ contributions at $n=5$, and become larger much faster as one goes to lower n. Even at $n=30$, where they are much smaller, they are still relatively large compared to the residual error using the $\nu=\pm 1/4$ terms. This behavior is in keeping with the nature of asymptotic expansions, where one is usually forced to just truncate at the smallest term. Unfortunately, this prevents us from analyzing the crossover region in $w(x)$ discussed by He and Vanderbilt in any quantitative detail. We take this situation as having hit the limit of value of the asymptotic expansion for $w(x)$, at least as far as we have carried it out (fourth-order energy expansion for μ). It is our belief at present that further quantitative improvements in agreement of the 1D theory of $w(x)$ with accurate computation would require refinements in the inversion of the function $\mu(E)$ and analytic continuation of $E(\mu)$.

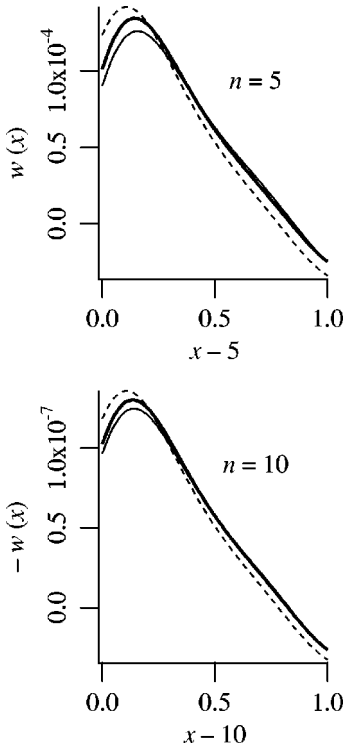

FIG. 7. Comparison of intermediate-n branches of the Wannier function calculated by wavelet methods (thick solid line) and by Fourier integration of the Bloch function in Eq. (30) using the $(\mu-\mu_0)^{-1/4}$ term (dashed line) and both the $(\mu-\mu_0)^{-1/4}$ and $(\mu-\mu_0)^{1/4}$ terms (thin solid line).

VI. SUMMARY AND DISCUSSION

A wavelet method for calculation of Wannier functions has been introduced and applied to a model Gaussian-based periodic potential. This method is direct and calculates the Wannier function $w(x)$ and the associated energy components ε_n simultaneously through a low-order restarted-Lanczos-type procedure. The locality and orthogonality advantages of compact support wavelets allow sparse matrix-vector multiplications, and the individual iteration steps scale linearly with basis size. The flexibility of the wavelet basis has also allowed systematic pursuit of convergence with respect to both intercell truncation errors (also possible with less flexible bases) and intracell basis set refinement. The converged results have been checked against the refined asymptotic analyses recently provided by He and Vanderbilt,[10] prompting a detailed analysis of yet higher-order corrections that contribute in the incompletely asymptotic distance regimes. Analytical formulas are derived and analyzed for these higher-order corrections and compared with the accurate results from the numerical wavelet calculations.

Other methods can of course be used for the calculation of the Wannier function of a 1D model potential, e.g., numerical Fourier transformation of the Bloch function calculated via standard methods. The present iterative method can be extended to higher dimensions using product wavelet bases while still retaining the capability of sparse matrix-vector multiplications, however, and preliminary investigations are being carried out in 2D. This is relevant, for example, to crossed-beam optical trapping of alkali-metal atom Bose-Einstein condensates.[39] Nevertheless, by far the strongest interest in calculation of Wannier or Wannier-like functions lies in the electronic structure community, and so the question naturally arises as to the suitability of wavelet bases for quantum chemistry calculations. While it must be emphasized that this is not a central question of the current investigation, there is already a certain body of research on the topic. Calculations using nonorthogonal Mexican hat wavelets,[27] interpolets[40,41] Daubechies wavelets,[42,43] Alpert multiwavelets,[35] lifted wavelets,[28] etc., have appeared over

the last ten years and research is still continuing.[44] Use of the Alpert multiwavelets to systematically control basis set error in quantum chemistry calculations is, in fact, in active development at this time at Oak Ridge National Laboratory.[45] It is therefore at least fair to assume that the answer to this question will become clearer over the course of time.

It is also reasonable to ask what relevance the corrections to simple exponential decay has for *ab initio* Wannier functions for real systems such as 3D semiconductors and insulators. Just as the exponential decay was found to apply in higher dimensions,[9] it is to be expected that corrections exist as well. (A trivial example would be a multidimensional crystal with a potential allowing separation of variables,[46] for which the 1D results immediately apply to each coordinate.) The precise nature of these corrections for different lattice geometries, connected bands, bond hybridization, and other complications remains to be determined, but already Taraskin *et al.*[11] have results in 1D, 2D, and 3D for a tight-binding insulator model on a simple cubic lattice. They find that the single-particle density matrix (which can be expanded in Wannier functions) decays with distance as $r^{-D/2}e^{-hr}$, agreeing in 1D with the results of He and Vanderbilt. In any event, it is reasonable to expect that the important regions in physical applications (e.g., insulator polarization[47]) will not be those in which the Wannier functions have decayed by 10–20 orders of magnitude, and therefore that there will be value in forcing future higher-dimensional asymptotic analyses to shorter distances (or at least to know the limiting factors in such pursuits). As mentioned in the Introduction, the much larger ideal goal with regard to *ab initio* calculations for real systems would seem to be a more global theory of Wannier functions which could aid in postanalysis of numerical results.

ACKNOWLEDGMENTS

Grateful acknowledgment is made for support of this work by National Science Foundation Grants No. CHE-0111008 and No. PHY-0139202 and by the Robert A. Welch Foundation.

[1] G. H. Wannier, Phys. Rev. **52**, 191 (1937).
[2] W. Kohn, Phys. Rev. **115**, 809 (1959).
[3] W. Kohn and J. R. Onffroy, Phys. Rev. B **8**, 2485 (1973).
[4] J. G. Gay and J. R. Smith, Phys. Rev. B **9**, 4151 (1974).
[5] V. V. Konotop, J. Opt. Soc. Am. B **14**, 364 (1997).
[6] D. Jaksch *et al.*, Phys. Rev. Lett. **81**, 3108 (1998).
[7] M. L. Chofalo, M. Polini, and M. P. Tosi, Eur. Phys. J. D **11**, 371 (2000).
[8] K. E. Strecker, G. B. Partridge, A. G. Truscott, and R. G. Hulet, Nature (London) **47**, 150 (2002).
[9] J. des Cloizeaux, Phys. Rev. **135**, A698 (1964).
[10] L. He and D. Vanderbilt, Phys. Rev. Lett. **86**, 5341 (2001).
[11] S. N. Taraskin, D. A. Drabold, and S. R. Elliott, Phys. Rev. Lett. **88**, 196405 (2002).
[12] N. Marzari and D. Vanderbilt, Phys. Rev. B **56**, 12 847 (1997).
[13] U. Stephan and D. A. Drabold, Phys. Rev. B **57**, 6391 (1998).
[14] U. Stephan, R. M. Martin, and D. A. Drabold, Phys. Rev. B **62**, 6885 (2000).
[15] T. Hoshi and T. Fujiwara, Surf. Sci. **493**, 659 (2001).
[16] I. Souza, N. Marzari, and D. Vanderbilt, Phys. Rev. B **65**, 035109 (2001).
[17] S. Goedecker, Rev. Mod. Phys. **71**, 1085 (1999).
[18] W. Kohn, Phys. Rev. B **7**, 4388 (1973).
[19] K. Kaneda and T. Odagaki, J. Phys. A **28**, 4389 (1995).
[20] I. Daubechies, *Ten Lectures on Wavelets* (SIAM Publications, Philadelphia, 1992).
[21] S. Mallat, *A Wavelet Tour of Signal Processing* (Academic Press, San Diego, 1998).
[22] J. P. Modisette, P. Nordlander, J. L. Kinsey, and B. R. Johnson, Chem. Phys. Lett. **250**, 485 (1996).
[23] P. Fischer, Int. J. Quantum Chem. **77**, 552 (2000).
[24] B. R. Johnson, J. L. Mackey, and J. L. Kinsey, J. Comput. Phys. **168**, 356 (2001).
[25] P. Fischer and M. Defranceschi, SIAM (Soc. Ind. Appl. Math.) J. Numer. Anal. **35**, 1 (1998).
[26] A. Maloney, J. L. Kinsey, and B. R. Johnson, J. Chem. Phys. **117**, 3548 (2002).
[27] K. Cho, T. A. Arias, J. D. Joannopolous, and P. K. Lam, Phys. Rev. Lett. **71**, 1808 (1993).
[28] S. Goedecker and O. V. Ivanov, Solid State Commun. **105**, 665 (1998).
[29] B. Poirier, J. Theor. Comput. Chem. **2**, 65 (2003).
[30] G. Parzen, Phys. Rev. **89**, 237 (1953).
[31] G. F. Koster, Phys. Rev. **89**, 67 (1953).
[32] P. O. Löwdin, J. Chem. Phys. **18**, 365 (1950).
[33] E. O. Kane and A. B. Kane, Phys. Rev. B **17**, 2691 (1978).
[34] C. K. Chui and J.-L. Lian, Appl. Numer. Math. **20**, 273 (1996).
[35] M. E. Brewster, G. I. Fann, and Z. Y. Yang, J. Math. Chem. **22**, 117 (1997).
[36] G. Beylkin, SIAM (Soc. Ind. Appl. Math.) J. Numer. Anal. **6**, 1716 (1992).
[37] B. R. Johnson, J. P. Modisette, P. J. Nordlander, and J. L. Kinsey, J. Chem. Phys. **110**, 8309 (1999).
[38] I. S. Gradshteyn and I. M. Ryzhik, *Table of Integrals, Series, and Products* (Academic, New York, 1965).
[39] M. D. Barrett, J. A. Sauer, and M. S. Chapman, Phys. Rev. Lett. **87**, 010404 (2001).
[40] R. A. Lippert, T. A. Arias, and A. Edelman, J. Comput. Phys. **140**, 278 (1998).
[41] T. A. Arias, Rev. Mod. Phys. **71**, 267 (1999).
[42] S. Wei and M. Y. Chou, Phys. Rev. Lett. **76**, 2650 (1996).
[43] C. J. Tymczak and X. Q. Wang, Phys. Rev. Lett. **78**, 3654 (1997).
[44] H.-J. Flad, W. Hackbusch, D. Kolb, and R. Schneider, J. Chem. Phys. **116**, 9641 (2002).
[45] G. I. Fann and R. Harrison (private communication).
[46] J. C. Slater, Phys. Rev. **87**, 807 (1952).
[47] I. Souza, T. Wilkens, and R. M. Martin, Phys. Rev. B **62**, 1666 (2000).